



# Effect of lateral stress on shear strength of jointed hard rocks in true triaxial single-shear test

Gang Wang<sup>1</sup> · Xia-Ting Feng<sup>1</sup> · Chengxiang Yang<sup>1</sup> · Jun Zhao<sup>1</sup> · Yongrun Xiong<sup>1</sup> · Jiarong Wang<sup>1</sup>

Received: 25 April 2023 / Accepted: 10 November 2023 / Published online: 27 November 2023  
© Springer-Verlag GmbH Germany, part of Springer Nature 2023

## Abstract

Shear failure along joints is one of the typical failure modes in deep underground rock masses, and indoor direct shear tests are commonly used to study the shear mechanical behavior of joints. However, deep underground rock masses are subjected to true triaxial stress conditions, and current indoor direct shear tests of joints only consider the shear stress and normal stress, without considering the influence of lateral stress. Therefore, in order to investigate the effect of lateral stress on the shear strength of jointed hard rocks, a series of true triaxial single-shear tests with different levels of lateral stress were conducted on intact hard rock, hard jointed rock (hard rock containing natural hard joints), and artificial jointed rock (hard rock containing open joints) using self-developed shear boxes and deformation measurement devices. The test results show that lateral stress can enhance the shear strength of intact granite and hard jointed granite but has little effect on that of artificial jointed granite. The shear strength of hard jointed granite is lower than that of intact granite and higher than that of artificial jointed granite. A simple linear function was used to describe the effect of lateral stress on the friction coefficients of these three types of specimens, and it was found that the enhancement effect of lateral stress on the friction coefficients of intact granite was greater than that on jointed granite. The failure mode of the specimens is jointly affected by normal stress, lateral stress, and joints. High normal stress and low lateral stress conditions often make the specimen prone to lateral peeling failure, and the presence of joints can reduce the lateral spalling failure of the specimen.

**Keywords** Jointed hard rock · Lateral stress · Shear strength · True triaxial single-shear test

## Introduction

The geological conditions of engineering rock masses involved in deep underground engineering construction tend to be complicated. In conditions of high geo-stresses, disasters caused by rock mass excavation and unloading occur frequently in deep underground engineering (Kaiser and Cai 2012; Liu et al. 2015; Feng et al. 2019; Huang et al. 2019; Zhao et al. 2022; Leng et al. 2023). In the process of deep underground engineering excavation, disasters are more likely to occur when deep underground caverns are close to geological discontinuities (Snelling et al. 2013; Hu et al.

2020). The shear failure of joints is a common fracture mode of rock masses (Barton 2013; Prassetyo et al. 2017; Du et al. 2022; Xue et al. 2023), and the strength of rock mass joints plays an important role in the safety analysis of the surrounding rock, so it is necessary to study the shear strength characteristics of joints through laboratory shear tests.

Following Mogi's (Mogi 1971) original work, scholars have realized that the intermediate principal stress will significantly affect the strength of rock under true triaxial compression (Ingraham et al. 2013; Ma and Haimson 2016; Zhang et al. 2019; Feng et al. 2021; Hu et al. 2023), and there are only few studies on the shear strength of rock joints under true triaxial single-shear conditions. Alan and Morris (2009), Kapang et al. (2013), and Wang et al. (2018) placed rectangular specimens with inclined cracks in true triaxial pressure chambers for shear tests. The lateral stress of each specimen was provided by oil pressure, and the shear stress and normal stress could be calculated by the applied  $\sigma_1$  and  $\sigma_2$ . However, during the application of  $\sigma_1$ , the normal force and shear force also changed,

✉ Xia-Ting Feng  
fengxiating@mail.neu.edu.cn

Jun Zhao  
zhaojun1@mail.neu.edu.cn

<sup>1</sup> Key Laboratory of Ministry of Education on Safe Mining of Deep Metal Mines, Northeastern University, Shenyang 110819, China

which might have affected the test results. Therefore, it is also necessary to conduct true triaxial single-shear tests on joints so that the application of normal force and shear force do not affect each other in the shear fracture process and more reasonable joint strength parameters can be obtained.

Joints are common discontinuities in deep engineering, and shear testing is the main method used to study the fracture process and strength of joints (Barton 2013; Zhang and Jiang 2020; Heng et al. 2022; Ban et al. 2023; Wu et al. 2023). Researchers have established various forms of shear strength models to study the shear strength of joints (Barton 2013; Muralha et al. 2014; Prasetyo et al. 2017; Liu et al. 2018; Li et al. 2020; Yang et al. 2020), and there are primarily two common approaches to investigate the shear strength of joints. One method is to obtain the trend of the peak shear strength of joints through a large number of shear tests, to explain the mechanical mechanism of shear strength. Another method mainly explains the mechanism of shear strength through theoretical analysis. Meng et al. (2017) employed dry soil, wet soil, and cement mortar particles as filling media to investigate the variations in the shear strength of filled rock joints under cyclic shear loading. They also conducted an analysis of the damage to filled joints during the shearing process using acoustic emission techniques. Shrivastava and Rao (2018) selected a mixture of hydrated gypsum, fine sand, and mica powder as the filling medium. They conducted direct shear tests on simulated serrated joints with varying initial roughness angles. This allowed them to establish a shear strength model for filled joints considering the effects of filling medium thickness and joint surface roughness under normal load and normal stiffness conditions. Zhao et al. (2021) have developed a novel natural rock joint strength model based on a fuzzy comprehensive evaluation of shear roughness classification methods. Their established strength model has been found to more comprehensively capture the influence of joint surface morphological parameters on shear strength and exhibits a good alignment with experimental data. In summary, many scholars have performed studies on the strength of joints and achieved good results. However, the direct shear testing of rock joints mostly adopts artificial joint specimens, and natural hard joints are rarely involved. This can be used to study the fracture process of artificial open joints, but it is necessary to further study the shear mechanical properties of hard joints.

To study the influence of lateral stress on the strength behavior and fracture process of rock joints, in this study, true triaxial single-shear tests were carried out on intact rock and hard jointed and artificial jointed hard rocks, and the strength law under true triaxial single-shear was proposed. Then, the influence of the shear strength of hard jointed rock under true triaxial stress on the failure of surrounding rock

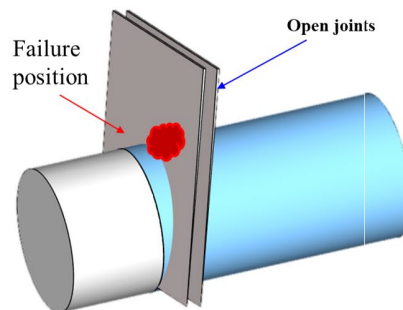
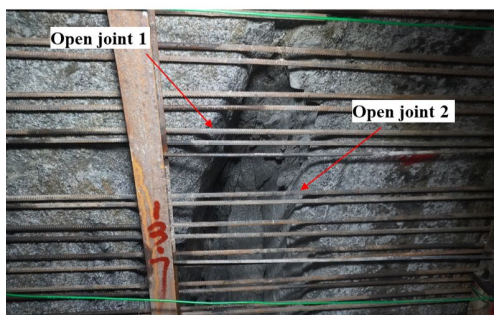
and the effect of lateral stress during the shear fracture process of hard jointed granite were discussed.

## Methodology and test procedures

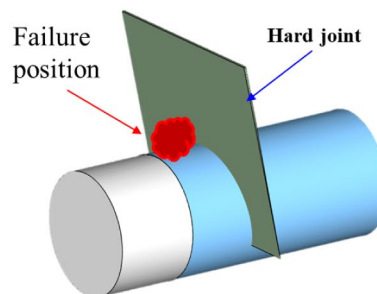
The existence of joints has a significant impact on the strength and deformation ability of rocks, failure in rock masses usually occurs along joints (Zhou et al. 2015; Sun et al. 2023), and joint-controlled failure is a typical disaster of deep tunnel projects (Fig. 1). A true triaxial single-shear test refers to the shear fracture test of a specimen under the combined action of lateral stress  $\sigma_p$ , normal stress  $\sigma_n$ , and shear stress  $\tau$ . In order to study the mechanical characteristics of joints, Northeast University of China has developed a shear box that can be used in conjunction with a true triaxial testing apparatus (Feng et al. 2018) to obtain the complete stress-strain curve of hard rock or jointed rock (Fig. 2). The shear force and normal force are directly applied by actuators, while the lateral stress is applied by hydraulic oil. Through sealant and sealing technology, direct contact between the specimen and hydraulic oil can be prevented, thus achieving three-dimensional stress application. A linear variable differential transformer (LVDT) is used to measure the deformation in the shear direction and normal direction, and a beam-type strain gauge is used to measure the deformation in the lateral direction.

Four kinds of hard rocks are selected for the true triaxial single-shear test, as shown in Fig. 3. Granite is taken from a tunnel construction site and sandstone from a quarry. The main purpose of this study is to analyze the effects of lateral stress and joint types on the shear strength of hard rock. The focus of the study is on granite, while sandstone is only used to verify the effect of lateral stress on the shear strength of intact granite. In order to reduce the impact of dispersion, rock specimens of the same type are all taken from the same rock block. After the rock specimens are made and naturally dried, rock specimens with small differences in density and wave velocity are selected for testing. The specific number of specimens and their stress conditions are shown in Table 1, where the wave velocity is the wave velocity of the specimen along the shear direction. The dimensions of the specimens are 70 mm × 70 mm × 70 mm. The sandstone bedding is set with its bedding perpendicular to the shear stress and treated as intact sandstone. The natural hard joints in granite are formed through the geological process of chloritization. These joints exist in a closed state and possess a certain tensile strength. Artificial jointed specimens (or can be referred to as artificial open jointed specimens) are created by shearing natural jointed granite until they reach the residual stage. To minimize the effects of specimen dispersion and maintain uniformity in joint parameters within the artificial joints, multistage loading tests were performed. Furthermore, to

**Fig. 1** Examples of typical disasters that occur in tunnel sections (the maximum horizontal principal stress is basically parallel to the tunnel axis): **a** collapse occurred at the right sidewall to the south spandrel where two open joints ( $305^\circ \angle 75^\circ$ ) can be seen; **b** rockburst occurred at the right spandrel to the vault where one hard joint ( $315^\circ \angle 75^\circ$ ) is apparent

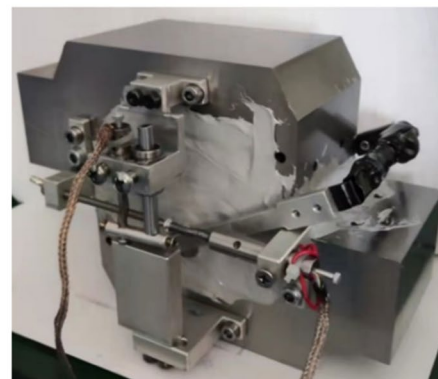
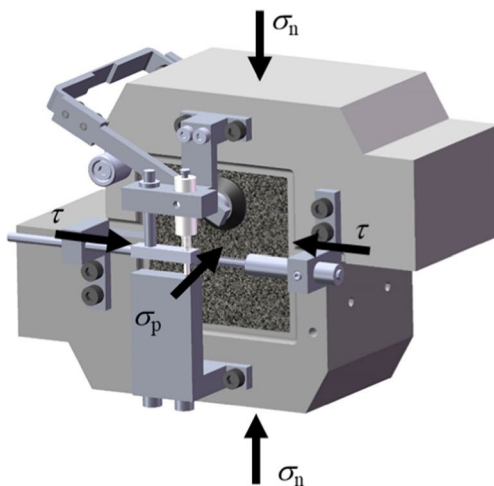


(a)



(b)

**Fig. 2** Shear box revised from Feng et al. (2021)



obtain comprehensive stress-strain curves, all other tests were conducted through single-shear procedures.

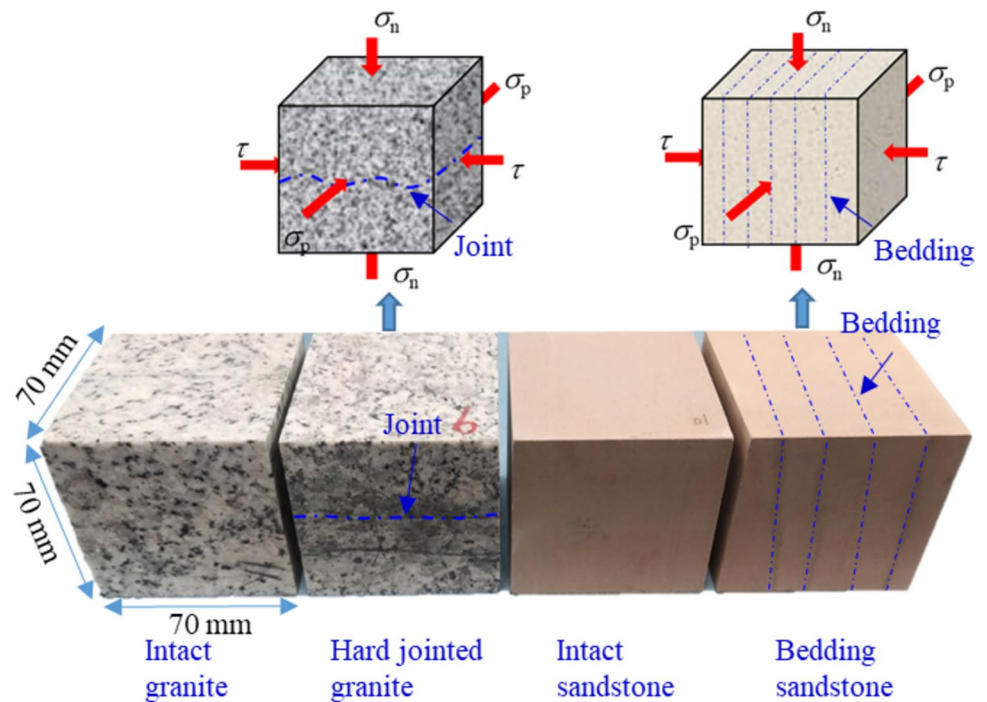
The specific test steps of the single-shear procedure are as follows (Feng et al. 2021):

- (a) The normal stress and lateral stress are applied by means of stress control until the target stress level is set.
- (b) The lateral stress remains unchanged, and the normal stress is applied independently until the set target stress level is reached.

- (c) Lateral stress and normal stress are held constant, while shear stress is applied through displacement control. When the specimen enters the residual strength stage (at which point the shear stress remains basically unchanged as the shear displacement increases), the test is stopped.

In multistage experiments, following the application of shear stress, continuous monitoring of the shear stress-shear displacement curve's slope is performed. When the slope

**Fig. 3** Four kinds of hard rock specimens



approaches zero, it is necessary to unload the shear force to approximately zero. Subsequently, in accordance with the experimental plan, changes in lateral stress or normal stress are introduced to predetermined levels, followed by the reapplication of shear force until the final stage of testing.

In addition, to verify the influence of lateral direction on the strength of specimens containing artificial joints, residual stage multistage true triaxial compression tests were conducted on three marble specimens using the method established by Wang et al. (2021). The dimensions of the specimens are 50 mm × 50 mm × 100 mm. After the true triaxial compression of the specimen to the residual stage, a macroscopic fracture surface has formed, which can be considered as a sample containing an artificial joint. The specific stress settings are shown in Table 2.

## Results and discussion

### Shear strength of intact rock

The relationship between the shear strength and lateral stress of intact hard rock (Fig. 4) shows that, within the test stress range, lateral stress and normal stress will enhance the peak shear strength of hard rock, and the peak shear strength of hard rock is more sensitive to normal stress than to lateral stress (Zhao et al. 2023). The role of the lateral stress in the true triaxial single-shear test is similar to that of the intermediate principal stress in the true triaxial compression test. The main reason is that the increase in the stress level leads

to the continuous reduction of the pores and gaps of the particles in the hard rock, increases the bite force between the particles in the rock, makes the hard rock denser, and requires greater stress to produce a new microfracture to improve the strength of the hard rock.

### Shear strength of jointed hard rock

Figure 5 shows the test curve of the hard jointed granite specimens under the true triaxial single-shear condition. The shear stress displacement curve of the specimen shows evident plastic deformation characteristics before the peak strength, and after the peak strength, except for the 0 MPa lateral stress condition, the first drop of the shear stress in the curve shows a brittle feature of sudden decrease in stress. This phenomenon happens because, although the local mineral particles in the specimen are damaged due to stress, the adjacent particles still have a certain bearing capacity, so the interaction and merging process of microfracture slows down, leading to an evident plastic deformation stage before the peak. In the displacement softening stage, except for the 0 MPa lateral stress condition, macroscopic fracture surfaces are formed, and some microconvex bodies in the specimen are suddenly cut and worn, resulting in normal compression deformation and a sudden decrease in shear force. When there is no lateral stress, due to the high normal stress (50 MPa), the specimen develops a splitting surface, perpendicular to the  $\sigma_p$  direction, from the stress surface of the  $\sigma_p$  to the interior of the specimen (Feng et al. 2021). Affected by

**Table 1** Test scheme for four types of hard rock used in true triaxial single-shear tests

Hard rock type	No.	Density (g/cm <sup>3</sup> )	Wave velocity (m/s)	$\sigma_n$ (MPa)	$\sigma_p$ (MPa)	Stress path
Intact granite	IG1	2.64	4207	30	0	Single-shear procedure
	IG2	2.63	4137	30	10	
	IG3	2.64	4235	50	0	
	IG4	2.64	3958	50	10	
	IG5	2.57	4026	50	30	
	IG6	2.63	4005	70	0	
	IG7	2.64	4120	70	10	
	IG8	2.66	4202	70	30	
	IG9	2.65	4200	70	50	
	IG10	2.63	4050	90	0	
	IG11	2.64	3995	90	10	
	IG12	2.65	4080	90	30	
Hard jointed granite	JG1	2.64	4317	30	0	
	JG2	2.63	4219	30	10	
	JG3	2.65	4640	30	20	
	JG4	2.63	4581	50	0	
	JG5	2.63	3648	50	10	
	JG6	2.61	4121	50	20	
	JG7	2.62	4113	50	30	
	JG8	2.64	4217	60	0	
	JG9	2.64	4644	60	10	
	JG10	2.63	3929	60	20	
	JG11	2.63	4211	60	30	
Intact sandstone	IS1	2.23	2383	30	0	
	IS2	2.20	2395	30	5	
	IS3	2.22	2428	30	10	
	IS4	2.16	2404	30	20	
	IS5	2.17	2169	20	0	
	IS6	2.16	2161	20	10	
	IS7	2.16	2195	20	20	
	IS8	2.16	2189	10	0	
	IS9	2.16	2251	10	5	
Bedding sandstone	BS1	2.12	2052	50	0	
	BS2	2.11	2051	50	15	
	BS 3	2.11	2040	50	30	
Artificial jointed granite	AG1	2.63	4327	50	0 → 10 → 20 → 30	Multistage shear procedure
	AG2	2.63	4321	50	10 → 20 → 30	
	AG3	2.65	4330	30	5 → 10 → 15 → 20	
	AG4	2.63	4401	30	10 → 15 → 20	
	AG5	2.64	4350	30	0 → 5 → 10	

this, the upper and lower shear fracture surfaces will produce mutually embedded convex bodies, which further promotes the development of fractures perpendicular to the  $\sigma_p$ . Therefore, in the postpeak stage, the normal direction is always shear shrinkage, and there is a large lateral expansion deformation. The application of lateral stress

promotes normal shear expansion deformation and inhibits the lateral expansion deformation of the specimens.

Figure 6 shows the test curve of artificial jointed granite specimens under true triaxial single-shear, with each stage of the test treated as a separate test. With increasing lateral stress, the deformation of the specimen at the unloading

**Table 2** Test scheme for residual stage multistage true triaxial compression test of marble specimens

No.	Density (g/cm <sup>3</sup> )	Wave velocity (m/s)	$\sigma_2$ (MPa)	$\sigma_3$ (MPa)
M1	2.82	4172	30 → 40 → 65	10
M2	2.82	4165	30 → 40 → 65	25
M3	2.82	4170	30 → 40 → 65	30

point (considered as the peak stress point) decreases, but the peak shear strength remains basically unchanged (Fig. 6a). This phenomenon can be attributed to the elevation of lateral stress, coupled with the loading and unloading cycle instigating plastic deformation at the fracture surface. This

process results in localized hardening, consequently diminishing the material’s deformation capacity. Nevertheless, owing to the inherent structural strength constraints at the fracture surface during the specimen’s shear slip process, the overall strength remains consistently stable. The peak normal dilatation deformation of the specimen shows an increasing trend, while the peak lateral dilatation deformation of the specimen shows a decreasing trend (Fig. 6b, c). This is because, after the application of lateral stress, the lateral compression of the specimen increases, resulting in a decrease in lateral deformation capacity, resulting in the deformation of the specimen mainly occurring along the normal direction.

The peak shear strength of hard rock with a joint under true triaxial single-shear is closely related to  $\sigma_p$  and the

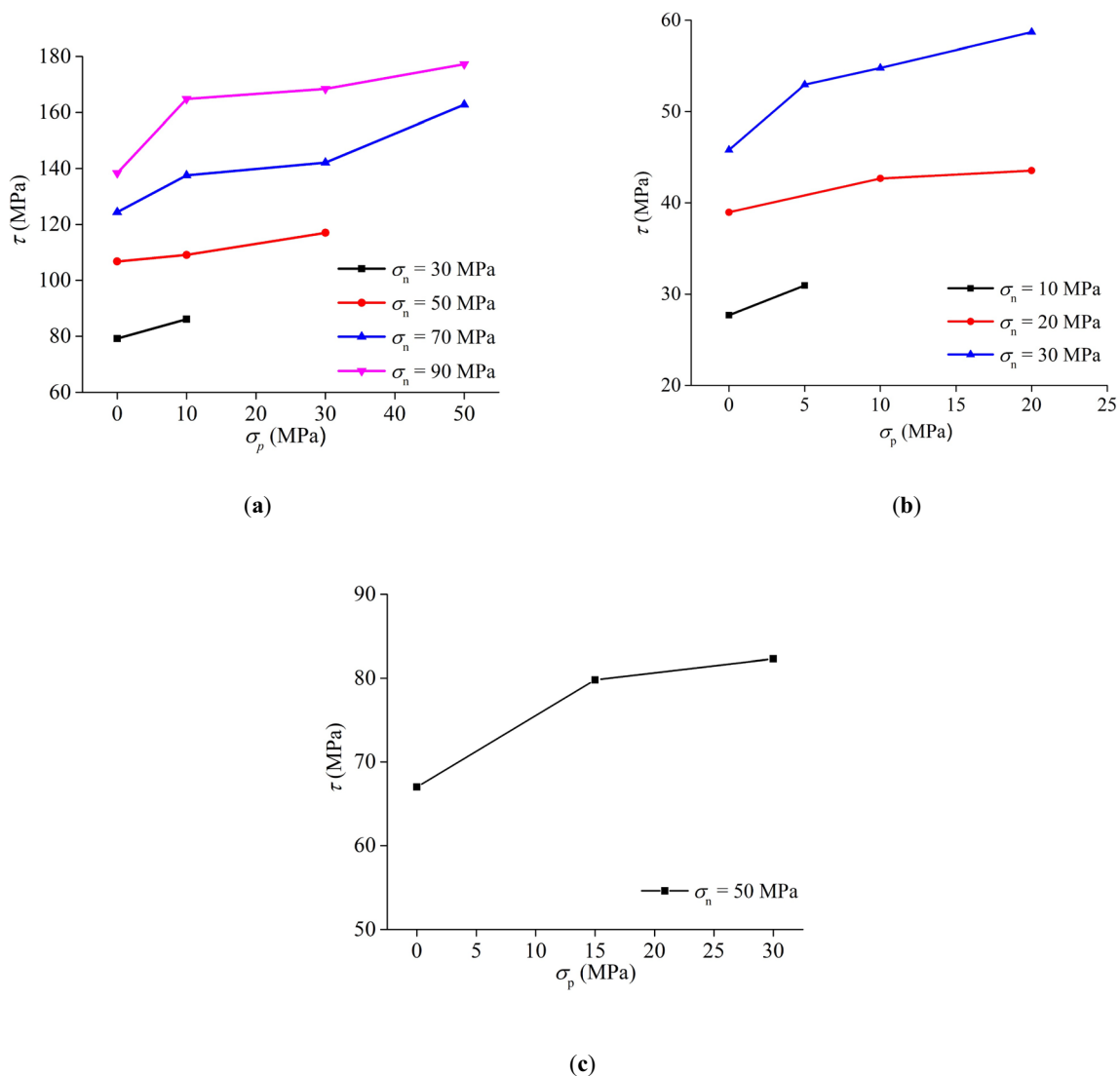
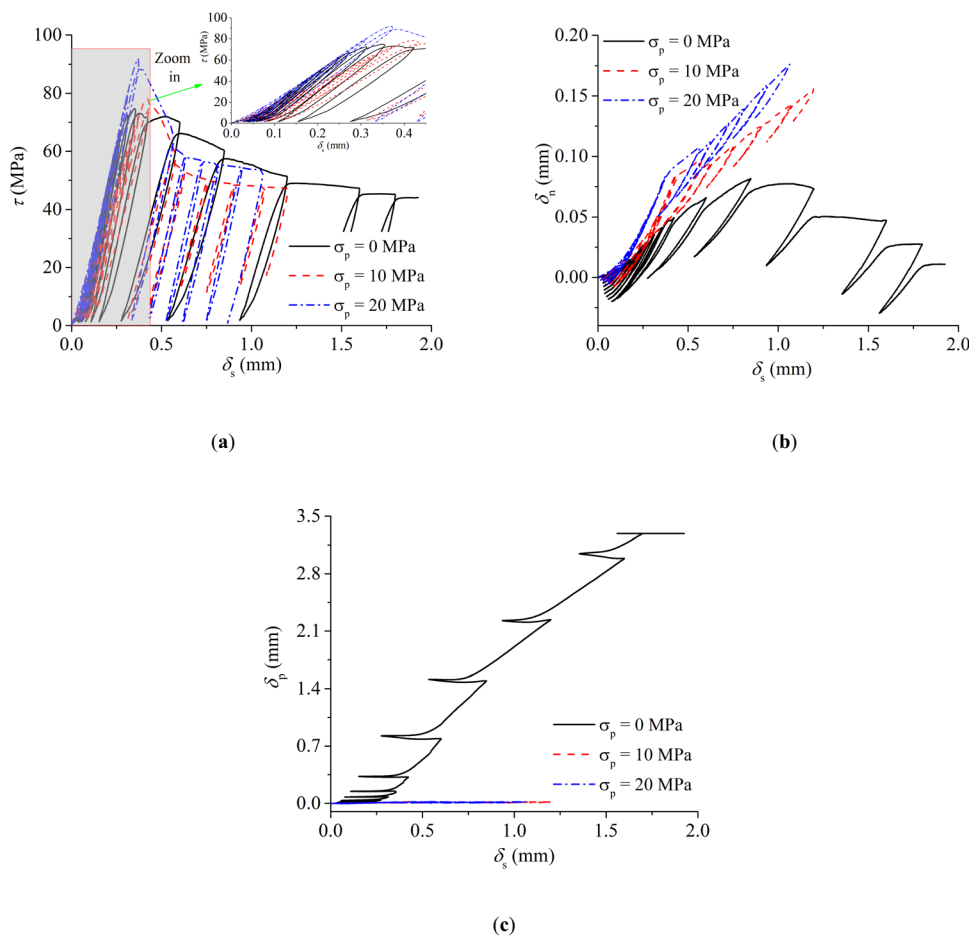


**Fig. 4** Relationship between the shear strength and lateral stress of intact hard rock: **a** intact granite; **b** intact sandstone (Feng et al. 2021); **c** bedding sandstone

**Fig. 5** Test results of hard jointed granite ( $\sigma_n = 50$  MPa): **a** the shear stress versus shear displacement curve; **b** the normal displacement (the positive direction is dilatancy) versus shear displacement curve; **c** the lateral displacement (the positive direction is dilatancy) versus shear displacement curve



joint strength. In the tested range of stresses, with the increase in lateral stress, the shear strength of natural jointed granite increases approximately linearly, while the shear strength of granite with artificial joints remains approximately unchanged. The peak shear strength of granite with natural joints is higher than that of granite with artificial joints (Fig. 7).

Similarly, in the true triaxial compression test of hard rock, the intermediate principal stress affects the peak strength of intact hard rock, but when the fracture of hard rock reaches the residual stage, increasing the intermediate principal stress does not affect the residual strength of hard rock (Fig. 8). This is because the macrofracture surface of the hard rock has been completely formed in the residual stage. In the residual stage, the strength of hard rock is mainly related to the relative sliding shear friction along the fracture surface. The intermediate principal stress is parallel to the fracture surface and will not change the sliding friction resistance, so it will not affect the residual strength.

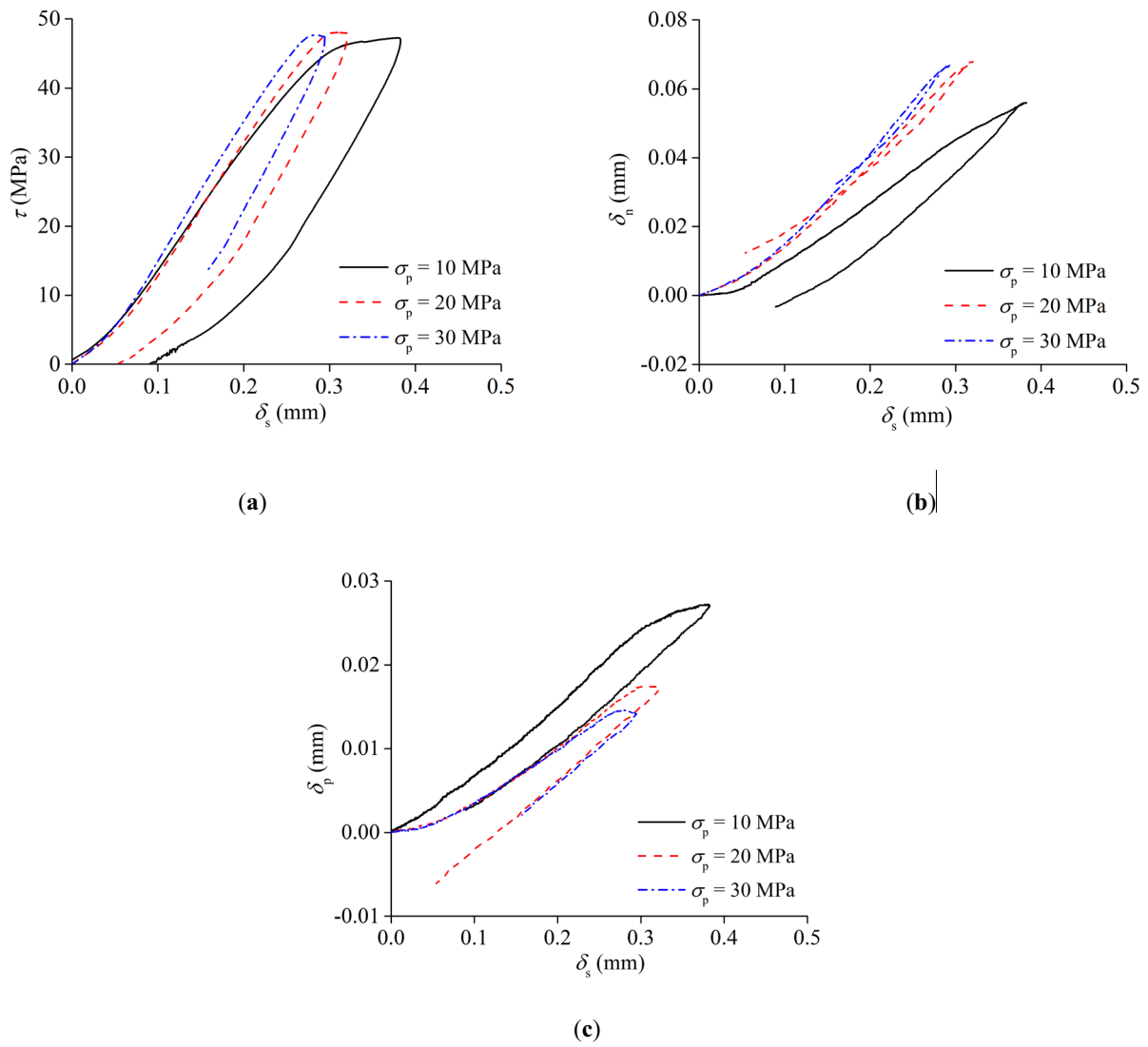
**Effect of  $\sigma_p$  on the friction coefficient**

To quantitatively characterize the effect of  $\sigma_p$  on the shear strength of different specimens, a simple linear function is adopted to describe the lateral stress effect on the friction coefficient ( $\tau/\sigma_n$ ) in three kinds of hard rocks:

$$\frac{\tau}{\sigma_n} = A\sigma_p + B \tag{1}$$

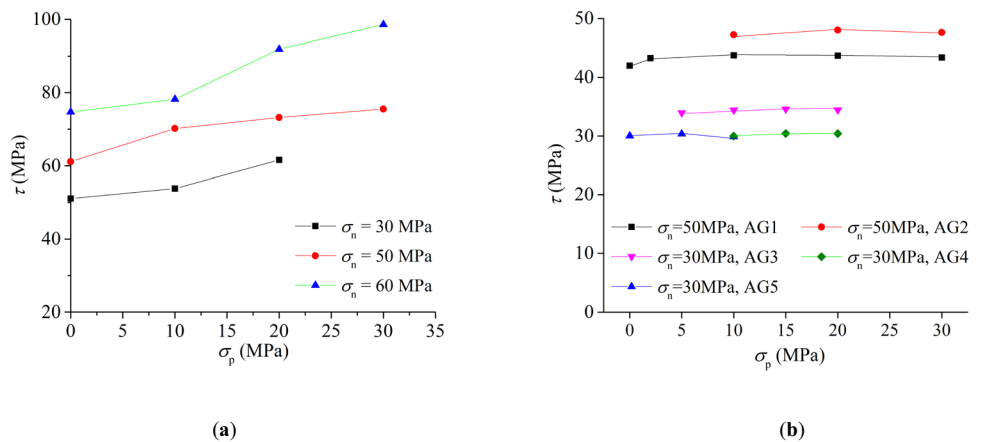
where  $\tau$ ,  $\sigma_n$ , and  $\sigma_p$  are the shear stress, normal stress, and lateral stress, respectively, and  $A$  and  $B$  are fitting coefficients.

Figure 9 shows the relationship between the friction coefficient and  $\sigma_p$  of different specimens. The friction coefficient of the artificial jointed specimens remains unchanged, while the friction coefficient of the intact specimens and natural jointed specimens increases linearly with increasing lateral stress. By using Eq. 1 to fit the data in Fig. 9, the fitting parameters shown in Table 3 can be obtained. Intact hard rock can be considered as a structural equivalent to specimens containing joints with joint



**Fig. 6** Test results of artificial jointed granite: **a** the shear stress versus shear displacement curve; **b** the normal displacement (the positive direction is dilatancy) versus shear displacement curve; **c** the lateral displacement (the positive direction is dilatancy) versus shear displacement curve

**Fig. 7** Relationship between the shear strength and lateral stress of jointed rock: **a** hard jointed granite and **b** artificial jointed granite





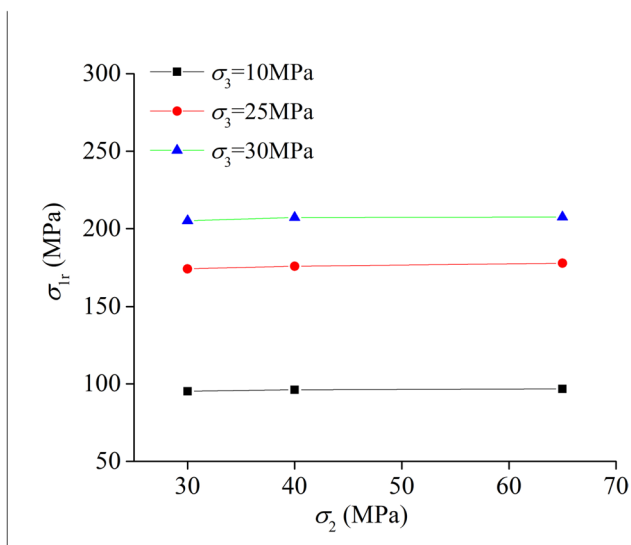


**Fig. 8** Effect of intermediate principal stress on residual strength of marble under true triaxial compression

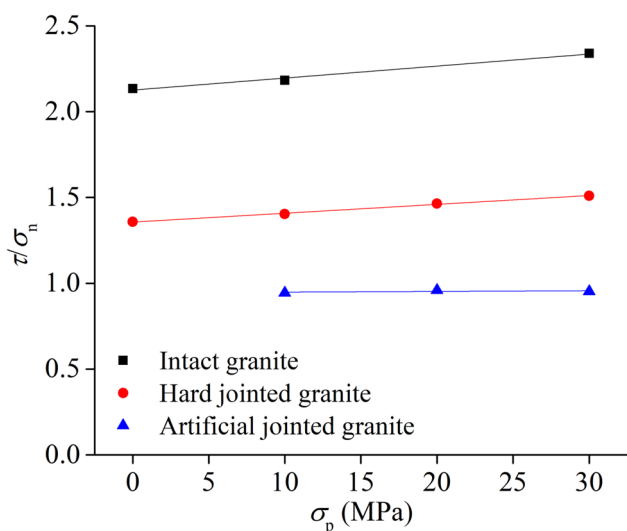


**Fig. 9** Relationship between the friction coefficient and lateral stress of different specimens

strength matching the intact material. Hard jointed rock specimens possess a certain strength, albeit lower than

**Table 3** The fitting parameters for different hard rock

Parameter	Rock type		
	Intact granite	Hard jointed granite	Artificial jointed granite
A	0.007	0.005	0
B	2.13	1.36	0.95

that of intact hard rock, due to the presence of hard joints. In contrast, artificial jointed specimens exhibit the lowest strength as the structural surfaces within them have fully opened. In intact hard rock, an increase in lateral stress can induce microscopic displacements among rock particles, leading to an expanded contact surface area between these particles. This consequently amplifies frictional resistance, resulting in an elevation of the friction coefficient. Within hard rock containing hard joints, the presence of these structural surfaces disrupts the prevailing frictional mechanisms. The influence of increased lateral stress on the enhancement of the friction coefficient on these surfaces may be subject to constraints imposed by the inherent characteristics of the hard joints themselves. In hard rock containing artificial joints, the structural surfaces have achieved complete separation, indicating that the frictional mechanisms within the specimen are primarily governed by the characteristics of the structural surfaces. As the structural surfaces are fully open, the impact of increased lateral stress on the enhancement of the friction coefficient on these surfaces is relatively minor, given that the structural surfaces have already reached maximum separation. The table (Table 3) shows that the values of A and B decrease gradually from intact granite to hard jointed granite and further to artificial jointed granite.

The expression for the three-dimensional linear failure criterion of deep hard rock (3DHRFC) proposed by Feng et al. (2020) is given by the following:

$$\begin{aligned} & (\sqrt{1-b+sb^2} + t(1-\sqrt{1-b+b^2}) \sin \varphi_0)(\sigma_1 - \sigma_3) \\ & = (\sigma_1 + \sigma_3) \sin \varphi_0 + 2c_0 \cos \varphi_0 \end{aligned} \tag{2}$$

where *b* is the constant intermediate principal stress coefficient,  $b = \frac{\sigma_2 - \sigma_3}{\sigma_1 - \sigma_3}$ ; *c*<sub>0</sub> and  $\varphi_0$  represent the cohesion and internal friction angle of rocks at *b* = 0, respectively; and *s* and *t* are material constants.

According to the Mohr circle characteristics of rock peak failure strength under constant stress Lode angle (or intermediate principal stress coefficient), as shown in Fig. 10a, the criterion form can be transformed into the following:

$$\tau = \sigma_n \tan \varphi_b + c_b \tag{3}$$

$$c_b = c_0 \cot \varphi_0 \tan \varphi_b \tag{4}$$

where *c*<sub>*b*</sub> and  $\varphi_b$  are the cohesion and internal friction angle at different *b* values, respectively.

Then, the shear mechanics criterion considering lateral stress can be written as follows:

$$\tau = \sigma_n \tan \varphi_p + c_p \tag{5}$$

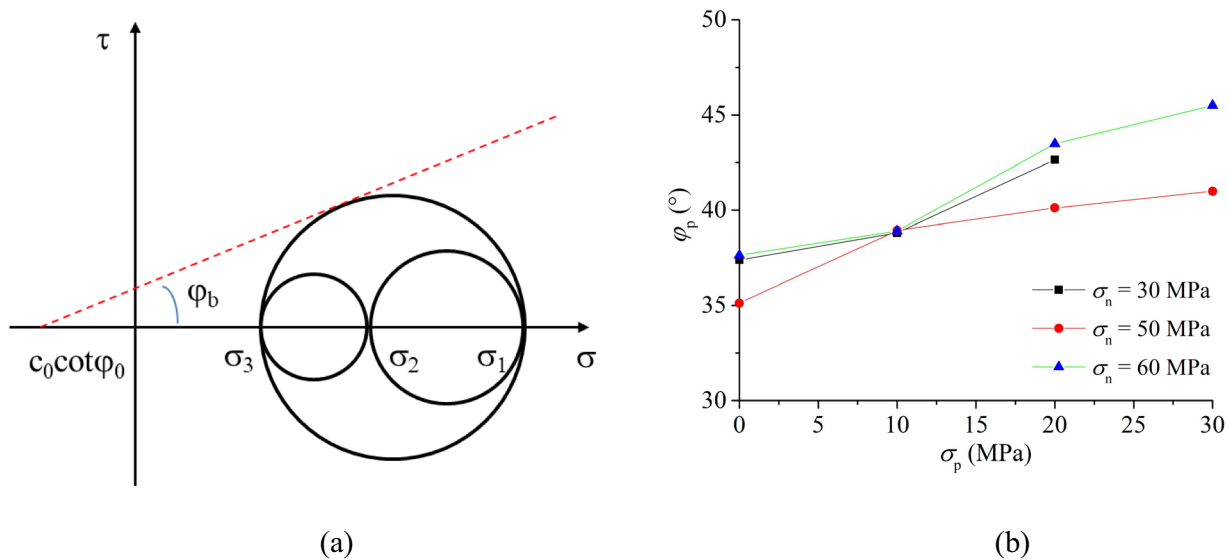


**Fig. 10** Mohr circle characteristics of rock peak failure strength: **a** Mohr circle of peak failure strength of rock (Feng et al. 2020) and **b** the relationship between  $\phi_p$  and  $\sigma_p$  of hard jointed granite

$$c_p = c_{s0} \cot \phi_{s0} \tan \phi_p \tag{6}$$

where  $c_{s0}$  and  $\phi_{s0}$  are the cohesion and internal friction angle at  $\sigma_p = 0$ , respectively, and  $c_p$  and  $\phi_p$  are the cohesion and internal friction angle at different  $\sigma_p$  values, respectively.

Combining Eqs. 4 and 5, we can obtain the following:

$$\tau = (\sigma_n + c_{s0} \cot \phi_{s0}) \tan \phi_p \tag{7}$$

From Eq. 7, we know that  $\tau$  increases with increasing  $\tan \phi_p$ . When the cohesion of the specimen is considered constant, the trend of the friction coefficient should be consistent with that of  $\tan \phi_p$ . Through Eq. 7 and experimental data, the relationship between lateral stress and  $\tan \phi_p$  can be obtained (Fig. 10b). From the figure, it can be seen that the  $\tan \phi_p$  shows an increasing trend with the increase of lateral stress.

### Failure characteristics

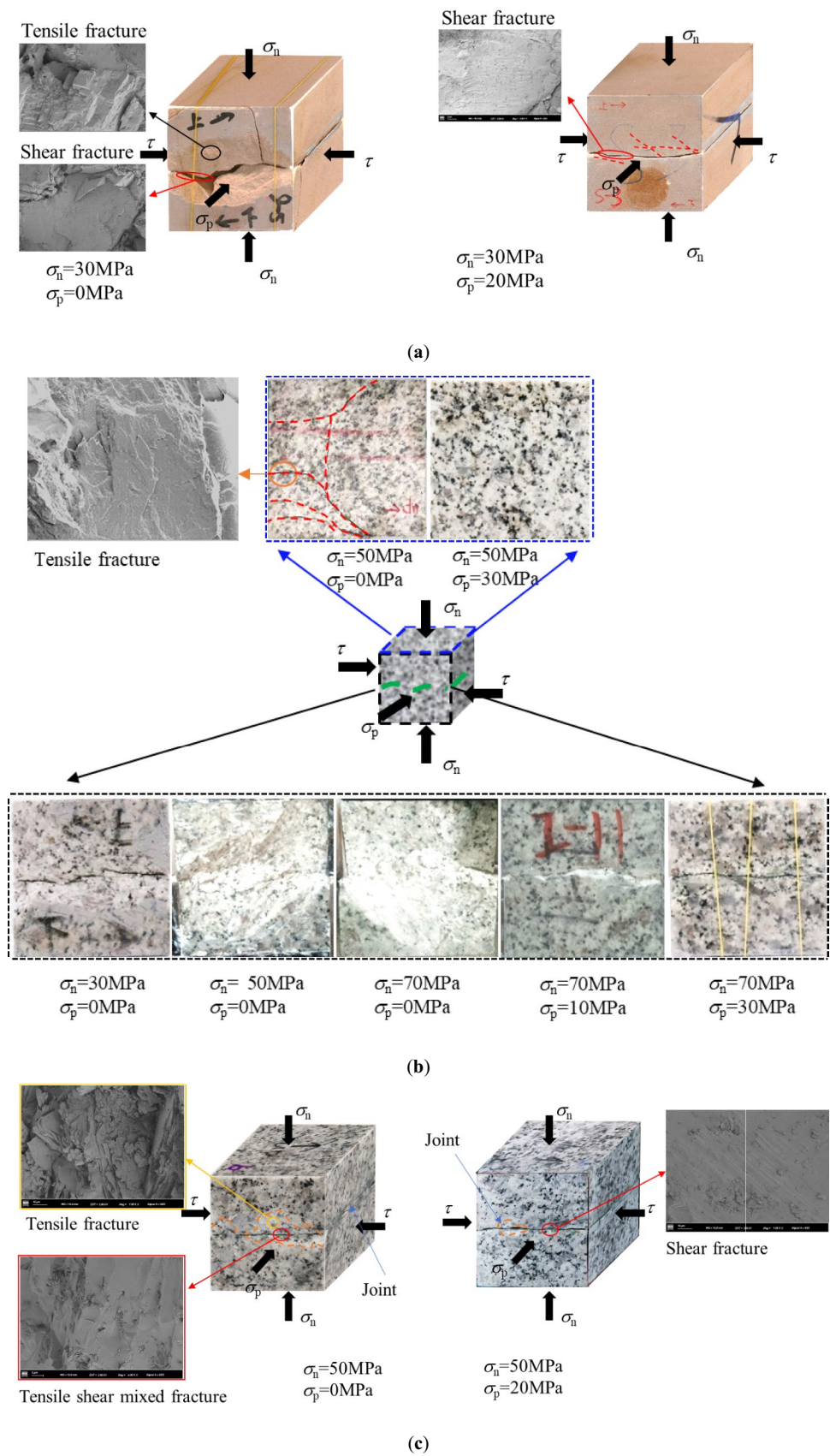
Figure 11 shows the shear failure patterns and partial fracture mechanisms of three types of hard rock specimens. It is evident that both normal stress and lateral stress have a significant influence on the macroscopic failure mode of the intact hard rock and the hard jointed rock specimens. When the lateral stress is relatively small, the lateral expansion deformation of intact sandstone specimens is more significant under the combined effect of shear force and normal force. As a result, fracture surfaces parallel to the plane where the shear force and normal force are

situated (tensile fracture mechanism) are produced, resulting in the “interlocking phenomenon” of the upper and lower shear fracture surfaces. The occurrence of these cracks reduces the shear resistance of the specimens, thereby decreasing their shear strength. Once the lateral stress is augmented, the lateral deformation of the specimens is restricted. Suppression of the development of fracture surfaces parallel to the plane where the shear force and normal force are located takes place. However, secondary cracks are produced near the main fracture surface of the specimens as the intact rock near the main fracture surface is subjected to shear force during the loading process. This leads to crack initiation and extension in various directions during the shearing process.

The failure pattern of the granite specimens reveals that when no lateral stress is applied, the lateral empty surface of the specimen undergoes block falling and peeling near the shear plane (tensile fracture mechanism), and the shear plane near the free surface has a considerable undulation. Upon increasing the normal stress, the area of lateral peeling increases gradually, and the specimen can be divided into multiple fragments by parallel fracture surfaces located in the plane of shear force and normal force, whose upper and lower parts are prone to interlock with each other. This lateral peeling decreases the effective shear area, leading to a decrease in the shear strength of the specimen. Additionally, as the lateral stress increases, the area of lateral peeling gradually reduces, and the shear plane becomes smoother.

Figure 11c depicts the shear failure mechanism of a granite specimen containing a hard joint. It is evident that when

**Fig. 11** Shear failure diagrams of three types of specimens: **a** intact sandstone; **b** intact granite; **c** hard jointed granite



subjected to no lateral stress, the specimen still experiences fragmentation and peeling in close proximity to the shear plane. However, this occurrence is significantly lesser as compared to that of intact hard rock. This is due to the fact that during the shearing process, the strength of the hard joint is lower than that of the surrounding hard rock. However, it still possesses a certain degree of strength. Therefore, the shearing force predominantly acts on the rock near the joint plane, resulting in a smaller shear body than that of intact hard rock. Based on the scanning results of the electron microscope (SEM) shown in Fig. 11c, the fracture surface of the lateral exfoliation area of the specimen exhibits characteristics of a significant tensile fracture mechanism, while on the shear surface, the dominant form of microfracture is shear fracture mechanism.

## Discussion

The shear fracture zone of intact and natural hard jointed specimens shows a certain width along the main fracture surface, which is manifested in the shear localization zone in the center of the specimen. The artificial jointed specimens were obtained from the residual stage of shear failure experiments, at which point the macroscopic shear fracture surface had been completely formed. Then, the stress state of the specimens was altered, and multistage loading experiments were conducted. Therefore, under this condition, the shear strength of specimens was mainly related to the friction

resistance of the fracture surface. Figure 12 shows the fracture process of hard jointed granite in the shear test and also presents the results of fracture type determination using the acoustic emission parameter feature discrimination method using the ratio of average frequency AF (the ratio of acoustic emission count to duration) to RA value (the ratio of acoustic emission rise time to amplitude). Since the hard joint has a certain tensile strength, before the unstable crack growth stage, the shear localization zone bears three-dimensional stress. Due to the anisotropy of the fracture (Feng et al. 2019), the cracks (tensile fracture and shear fracture) are distributed in the entire shear localization area and contain microcracks, perpendicular to  $\sigma_p$ . At this time, the lateral stress will increase the shear strength of the specimen. At the stage of unstable crack growth, the crack starts to propagate along the joint; the role of lateral stress decreases gradually, until the macroscopic fracture surface forms; and the lateral stress basically loses its role. Therefore, the lateral stress can promote the increment of shear strength of hard jointed granite but insignificantly affect the shear strength of artificial open jointed granite.

The deep hard rock is in a three-dimensional stress state, and the lateral stress has different effects on the shear strength of different types of joints. When analyzing the strength of joints in deep engineering, the influence of lateral stress may not be considered for open joints (similar to artificial joints) with a high degree of development (tensile strength equal to 0 MPa). Hard joints of deep engineering are closed, with no filling or high-strength microfilling

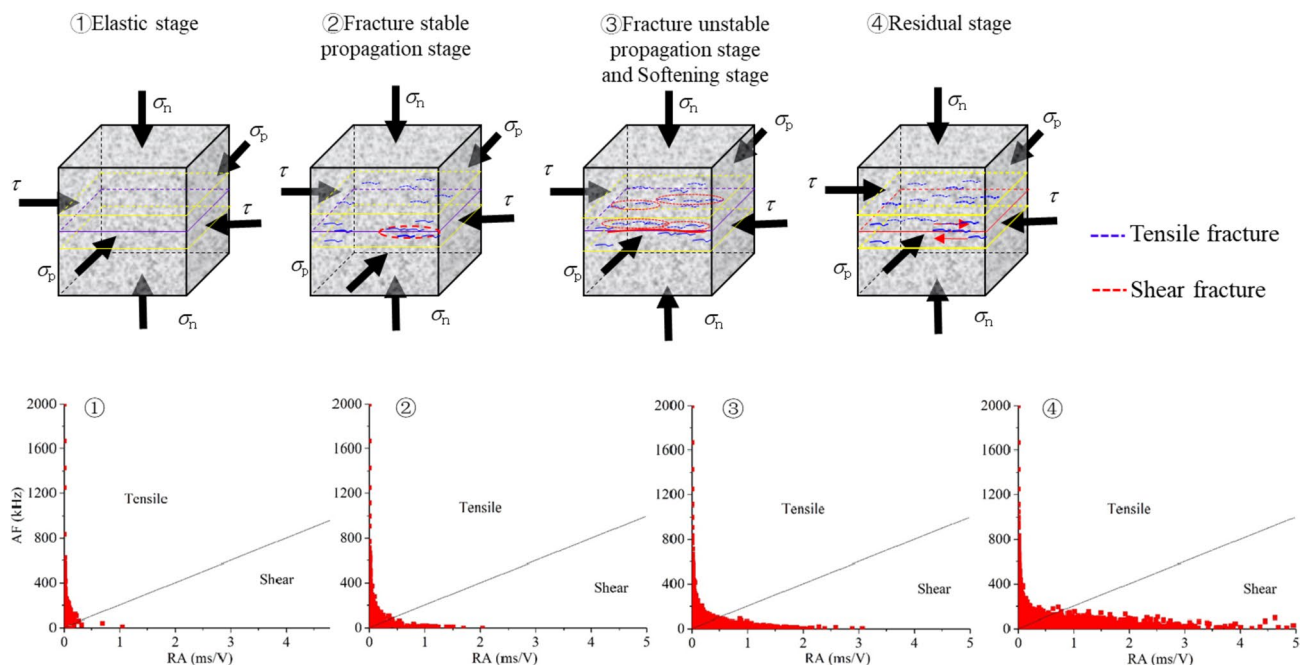


Fig. 12 Fracture process of hard jointed granite in shear test

inside, and have a certain tensile strength (Gao et al. 2020; Hu et al. 2020). The shear strength of the hard jointed specimens obtained from the conventional direct shear test is lower than the true triaxial single-shear test value under the same  $\sigma_n$ . Before the hard joint is cut off, energy is continuously accumulated under the action of stress. The accumulation of energy is related to the strength of the joint: the higher the strength, the more energy is accumulated. When the external force is enough to overcome the shear strength of the joint, the joint in the original equilibrium state is cut off instantly, releasing great energy, and the rock mass vibrates, causing the rock slab or rock block, cracked at the boundary of the tunnel, to eject, resulting in disasters. If the lateral stress effect of the shear strength of hard joints is not considered, the grade of a shear disaster may be underestimated. When conducting simulation calculations for tunnels containing hard joints, the neglect of lateral stress effects can potentially lead to lower calculated shear strength values based on the hard joint's strength criteria. Additionally, the energy release at the hard joint during failure tends to be relatively lower in such cases. This situation could result in a broader simulated zone of damage with relatively less severe degrees of damage.

## Conclusions

To study the effect of lateral stress on the shear strength of jointed hard rocks, true triaxial single-shear tests were carried out on different hard rocks. The main conclusions are as follows:

- (1) Lateral stress has varying effects on the shear strength of different types of granite. Specifically, lateral stress can increase the shear strength of intact granite and hard jointed granite, while its influence on the shear strength of artificial jointed granite can be neglected.
- (2) The shear strength of intact granite is higher than that of hard jointed granite, and both exhibit higher shear strength than artificial jointed granite. A simple linear function is utilized to describe the impact of lateral stress on the friction coefficient of these three types of specimens. The increase in lateral stress has a significantly greater effect on the friction coefficient of intact granite compared to hard jointed granite, while it has minimal impact on the friction coefficient of artificial jointed granite.
- (3) In the absence of lateral stress and under significant normal stress, hard rock specimens are prone to experience lateral spalling failure, leading to substantial lateral deformation. However, the application of lateral stress restricts the lateral deformation capacity of the specimens, reducing the extent of lateral spalling zones.

The presence of hard joints can concentrate fractures at the joint surfaces, thereby mitigating lateral spalling failure of the specimens.

**Funding** The authors gratefully acknowledge the financial support from the National Natural Science Foundation of China (Grants 51839003 and 52209125).

## Declarations

**Conflict of interest** The authors declare no competing interests, and all data used during the study appear in the published article.

## References

- Alan P, Morris DA (2009) The importance of the effective intermediate principal stress ( $\sigma_2$ ) to fault slip patterns. *J Struct Geol* 31(9):950–959. <https://doi.org/10.1016/j.jsg.2008.03.013>
- Ban L, Tao Z, Du W, Hou Y (2023) A consecutive joint shear strength model considering the 3D roughness of real contact joint surface. *Int J Min Sci Technol* 33(5):617–624
- Barton N (2013) Shear strength criteria for rock, rock joints, rockfill and rock masses: problems and some solutions. *J Rock Mech Geotech Eng* 5:249–261. [https://doi.org/10.1007/978-3-642-32814-5\\_1](https://doi.org/10.1007/978-3-642-32814-5_1)
- Du S, Lin H, Yong R, Liu G (2022) Characterization of joint roughness heterogeneity and its application in representative sample investigations. *Rock Mech Rock Eng* 1-25:3253–3277. <https://doi.org/10.1007/s00603-022-02837-4>
- Feng XT, Kong R, Yang C, Zhang X, Wang Z, Han Q, Wang G (2020) A three-dimensional failure criterion for hard rocks under true triaxial compression. *Rock Mech Rock Eng* 53:103–111. <https://doi.org/10.1007/s00603-019-01903-8>
- Feng XT, Kong R, Zhang X, Yang C (2019) Experimental study of failure differences in hard rock under true triaxial compression. *Rock Mech Rock Eng* 52:2109–2122. <https://doi.org/10.1007/s00603-018-1700-1>
- Feng XT, Wang G, Zhang X, Yang C, Kong R, Zhao J, Xu H (2021) Experimental method for direct shear tests of hard rock under both normal stress and lateral stress. *Int J Geomech* 21:04021013. [https://doi.org/10.1061/\(ASCE\)GM.1943-5622.0001951](https://doi.org/10.1061/(ASCE)GM.1943-5622.0001951)
- Feng XT, Zhao J, Zhang X, Kong R (2018) A novel true triaxial apparatus for studying the time-dependent behaviour of hard rocks under high stress. *Rock Mech Rock Eng* 51:2653–2667. <https://doi.org/10.1007/s00603-018-1516-z>
- Gao Y, Feng XT, Wang Z, Zhang X (2020) Strength and failure characteristics of jointed marble under true triaxial compression. *Bull Eng Geol Environ* 79:891–905. <https://doi.org/10.1007/s10064-019-01610-2>
- Heng S, Guo Y, Li X, Zhao R (2022) Shear stress distribution in rock-cemented discontinuities under direct shear: theoretical analysis and numerical validation. *Int J Geomech* 2:22. [https://doi.org/10.1061/\(ASCE\)GM.1943-5622.0002233](https://doi.org/10.1061/(ASCE)GM.1943-5622.0002233)
- Hu L, Feng XT, Xiao Y, Wang R, Feng G, Yao Z, Zhang W (2020) Effects of structural planes on rockburst position with respect to tunnel cross-sections: a case study involving a railway tunnel in China. *Bull Eng Geol Environ* 79:1061–1081. <https://doi.org/10.1007/s10064-019-01593-0>
- Hu L, Yu L, Ju M, Li X, Tang C (2023) Effects of intermediate stress on deep rock strainbursts under true triaxial stresses. *J Rock Mech Geotech Eng* 15(3):659–682. <https://doi.org/10.1016/j.jrmge.2022.06.008>

- Huang JZ, Feng XT, Zhou YY (2019) Stability analysis of deep-buried hard rock underground laboratories based on stereophotogrammetry and discontinuity identification. *Bull Eng Geol Environ* 78:5195–5217. <https://doi.org/10.1007/s10064-019-01461-x>
- Ingraham MD, Issen KA, Holcomb DJ (2013) Response of Castlegate sandstone to true triaxial states of stress. *J Geophys Res Solid Earth* 118:536–552. <https://doi.org/10.1002/jgrb.50084>
- Kaiser PK, Cai M (2012) Design of rock support system under rockburst condition. *J Rock Mech Geotech Eng* 4:215–227. <https://doi.org/10.3724/SP.J.1235.2012.00215>
- Kapang P, Walsri C, Sriapai T, Fuenkajorn K (2013) Shear strengths of sandstone fractures under true triaxial stresses. *J Struct Geol* 48:57–71. <https://doi.org/10.1016/j.jsg.2012.12.007>
- Leng D, Shi W, Liang F, Li H, Yan L (2023) Stability and deformation evolution analysis of karstified slope subjected to underground mining based on Hoek–Brown failure criterion. *Bull Eng Geol Environ* 82(5):1–16. <https://doi.org/10.1007/s10064-023-03211-6>
- Li B, Ye X, Dou Z, Zhao Z, Li Y, Yang Q (2020) Shear strength of rock fractures under dry, surface wet and saturated conditions. *Rock Mech Rock Eng* 53:2605–2622. <https://doi.org/10.1007/s00603-020-02061-y>
- Liu J, Li Y, Xu S, Xu S, Jin C (2015) Cracking mechanisms in granite rocks subjected to uniaxial compression by moment tensor analysis of acoustic emission. *Theor Appl Fract Mech* 75:151–159. <https://doi.org/10.1016/j.tafmec.2014.12.006>
- Liu Q, Tian Y, Ji P, Ma H (2018) Experimental investigation of the peak shear strength criterion based on three-dimensional surface description. *Rock Mech Rock Eng* 51(4):1005–1025. <https://doi.org/10.1007/s00603-017-1390-0>
- Ma X, Haimson BC (2016) Failure characteristics of two porous sandstones subjected to true triaxial stresses. *J Geophys Res Solid Earth* 121:6477–6498. <https://doi.org/10.1002/2016JB013637>
- Meng F, Zhou H, Wang Z (2017) Influences of shear history and infilling on the mechanical characteristics and acoustic emissions of joints. *Rock Mech Rock Eng* 50(8):2039–2057. <https://doi.org/10.1007/s00603-017-1207-1>
- Mogi K (1971) Fracture and flow of rocks under high triaxial compression. *J Geophys Res* 76:1255–1269
- Muralha J, Grasselli G, Tatone B, Blümel M, Chryssanthakis P, Jiang YJ (2014) ISRM suggested method for laboratory determination of the shear strength of rock joints: revised version. *Rock Mech Rock Eng* 47:291–302. [https://doi.org/10.1007/978-3-319-07713-0\\_10](https://doi.org/10.1007/978-3-319-07713-0_10)
- Prasetyo SH, Gutierrez M, Barton N (2017) Nonlinear shear behavior of rock joints using a linearized implementation of the Barton–Bandis model. *J Rock Mech Geotech Eng* 9(4):671–682. <https://doi.org/10.1016/j.jrmge.2017.01.006>
- Shrivastava AK, Rao KS (2018) Physical modeling of shear behavior of infilled rock joints under CNL and CNS boundary conditions. *Rock Mech Rock Eng* 51(1):101–118. <https://doi.org/10.1007/s00603-017-1318-8>
- Snelling PE, Godin L, McKinnon SD (2013) The role of geologic structure and stress in triggering remote seismicity in Creighton Mine, Sudbury, Canada. *Int J Rock Mech Min Sci* 58:166–179. <https://doi.org/10.1016/j.ijrmms.2012.10.005>
- Sun X, Zhao W, Shen F (2023) Physical modelling of deformation and failure mechanisms and supporting effects for a deep-buried tunnel in inclined layered strata. *Bull Eng Geol Environ* 82:74. <https://doi.org/10.1007/s10064-023-03104-8>
- Wang G, Feng XT, Yang C (2021) Experimental study of the mechanical characteristics of Jinping marble under multi-stage true triaxial compression testing. *Rock Mech Rock Eng* 2:55. <https://doi.org/10.1007/s00603-021-02704-8>
- Wang G, Wang P, Guo Y, Li W (2018) A novel true triaxial apparatus for testing shear seepage in gas-solid coupling coal. *Geofluids* 1–9. <https://doi.org/10.1155/2018/2608435>
- Wu X, Zheng H, Jiang Y, Deng T, Xiao G, Wang Y (2023) Effect of cyclic shear loading on shear performance of rock bolt under different joint roughness. *Rock Mech Rock Eng* 56(3):1969–1980. <https://doi.org/10.1007/s00603-022-03174-2>
- Xue Y, Ban L, Du W et al (2023) Peak shear strength model considering the dilation and shear failure effect of actual contact joint asperities. *Bull Eng Geol Environ* 82:63. <https://doi.org/10.1007/s10064-023-03077-8>
- Yang H, Wang Y, Li J, Zhang B (2020) A method to determine the shear strength of structural plane based on energy conservation. *Chin J Rock Mech Eng* 39:2674–2682. <https://doi.org/10.13722/j.cnki.jrme.2019.0623>
- Zhang Y, Feng XT, Yang C, Zhang X, Sharifzadeh M, Wang Z (2019) Fracturing evolution analysis of Beishan granite under true triaxial compression based on acoustic emission and strain energy. *Int J Rock Mech Min Sci* 117:150–161. <https://doi.org/10.1016/j.ijrmms.2019.03.029>
- Zhang Y, Jiang YJ (2020) Shear behavior and acoustic emission characteristics of en-echelon joints under constant normal stiffness conditions. *Theor Appl Fract Mech* 109:102772. <https://doi.org/10.1016/j.tafmec.2020.102772>
- Zhao J, Feng XT, Guo H (2022) Time-dependent failure characteristics of excavated rock masses in deep buried engineering: a field case and experimental study. *Bull Eng Geol Environ* 81:520. <https://doi.org/10.1007/s10064-022-03026-x>
- Zhao J, Hu L, Feng XT (2023) Shear failure mechanisms of sandstone subjected to direct, true triaxial and confining shear test conditions. *Rock Mech Rock Eng* 56(9):6889–6903. <https://doi.org/10.1007/s00603-023-03410-3>
- Zhao Y, Zhang C, Wang Y, Lin H (2021) Shear-related roughness classification and strength model of natural rock joint based on fuzzy comprehensive evaluation. *Int J Rock Mech Min Sci* 137:104550. <https://doi.org/10.1016/j.ijrmms.2020.104550>
- Zhou H, Meng F, Zhang C (2015) Analysis of rockburst mechanisms induced by structural planes in deep tunnels. *Bull Eng Geol Environ* 74:1435–1451. <https://doi.org/10.1007/s10064-014-0696-3>

Springer Nature or its licensor (e.g. a society or other partner) holds exclusive rights to this article under a publishing agreement with the author(s) or other rightsholder(s); author self-archiving of the accepted manuscript version of this article is solely governed by the terms of such publishing agreement and applicable law.